

Stochastic Dynamics for Video Infilling

Qiangeng Xu¹ Hanwang Zhang² Weiyue Wang¹ Peter N. Belhumeur³ Ulrich Neumann¹
¹University of Southern California ²Nanyang Technological University ³Columbia University
 {qiangenx, weiyuewa, uneumann}@usc.edu hanwangzhang@ntu.edu.sg belhumeur@cs.columbia.edu

Abstract

This paper introduces a stochastic generation framework (SDVI) to infill long intervals in video sequences. Video interpolation aims to produce transitional content for a short interval between every two frames to increase the temporal resolution. Video Infilling, however, aims to infill long intervals in a video with a possible sequence. Our framework models the infilling as a constrained stochastic generation process and sequentially samples dynamics from the inferred distribution. SDVI consists of two parts: (1) a bi-directional constraint propagation to guarantee the spatial-temporal coherency among frames, (2) a stochastic sampling process to generate dynamics from the inferred distributions. Experimental results show that SDVI can generate clear and varied sequences. Moreover, motions in the generated sequences are realistic and able to transfer smoothly from the referenced start frame to the terminal frame. Full paper see <https://arxiv.org/pdf/1809.00263.pdf>

1. Introduction

Video temporal enhancement is generally achieved by synthesizing frames between every two consecutive frames in a video. To our best knowledge, most studies [3] focus on interpolating videos with frame rate above 20 fps. The between-frame intervals of these videos are short-term and suitable for interpolation methods. Instead, our study focuses on the **long-term interval infilling** for videos with frame rate under 3 fps. The applications of the study could be applied on low frame rate videos recorded by any camera with limited memory, storage, network bandwidth or low power supply (e.g., outdoor surveillance devices and webcam with an unstable network).

In Figure 1, conditioned on frame 7 and 8, interpolation for short-term intervals requires to generate transitional frames containing similar content. However, infilling a long-term interval (from frame 8 to 12) with a sequence requires to generate motion dynamics and varying content.

Figure 2 illustrates the stochastic nature of the long-term intervals. We observe the following two phenomena: (1) Compared with scenario 1, since both the interval length and the difference between the two reference frames are larger, the uncertainties in the long-term interval are greater. (2) Taken frame 5 and 9 as references, both motion 1 and 2 are possible. If we also add frame 1 and 13 as references, only motion 2 is plausible. Consequently, utilizing long-term information (frame 1 and 13 in Figure 2) can benefit the dynamics infer-

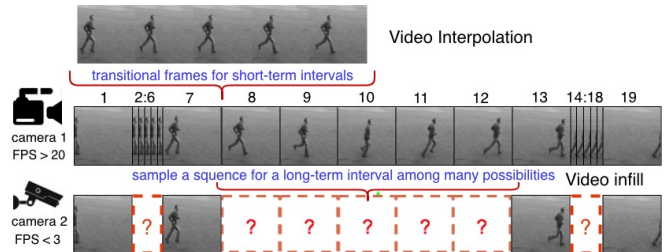


Figure 1: Task formulation: Camera 1 captures frames 1 to 19. Camera 2 only captures frame 1, 7, 13, 19.

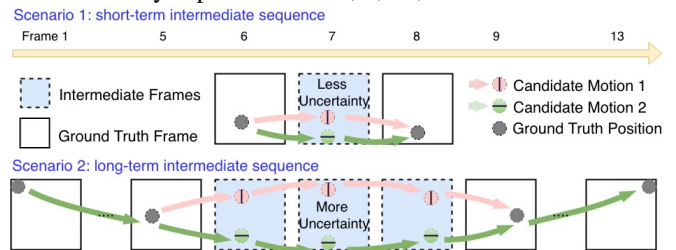


Figure 2: The difference of the stochasticity between short-term and long-term intervals. The red and the green trajectories indicate two possible motions in each scenario.

ence by eliminating uncertainties.

2. Task Formulation

For a sequence \mathbf{X} , only one out of every u frames ($u = T - S$) is captured. SDVI infills a sequence $\tilde{X}_{S+1:T-1}$ between reference frames X_S and X_T . In Figure 1, X_S and X_T are frame 7 and 13. We also use additional frames (frame 1 and 19) as extended references. X_S , X_T and extended reference frames (here we choose $i=1$) form the reference set “window of reference” \mathbf{X}_{WR} .

$$\underbrace{X_{S-i \times u}, \dots, X_{S-u}, X_S}_{\text{extended reference frames}}, \underbrace{\tilde{X}_{S+1:T-1}}_{\text{our target}}, \underbrace{X_T, X_{T+u}, \dots, X_{T+i \times u}}_{\text{extended reference frames}}$$

3. Model Overviews

Most video interpolation methods [5] rely on estimating the short-term pixel movements. While this approach falls short of long-term sequence generation, similar to the video prediction, we explicitly model the motion dynamics of the interval. The task has two major challenges:

1. The inputs of the video prediction are consecutive frames so the initial momentum is given. However, the inputs of infilling are sparse and discontinuous (X_S and X_T), which makes the task more challenging.
2. For infilling, the observation of the last frame becomes a

long-term requirement. Video prediction only generates visually plausible frames, while infilling also needs to satisfy the coherence with the terminal frame.

To inference the initial and final momentum, we expose extended reference frames both from the past (frame 1 and 7 in Figure 1) and the future (frame 13 and 19) to the model. To achieve the long-term coherence, we introduce a module *RBCConvLSTM*, a multi-layer bi-directional ConvLSTM with residual connections between adjacent layers. The dynamics from both sides are gradually propagated to the middle steps and create dynamic constraint vectors to guide the inference step by step.

To model the uncertainty of the intermediate sequences, we propose a stochastic generation model. The model first takes two reference frames and the extended reference frames to extract the dynamic features. Then we use the *RBCConvLSTM* to create constraint vectors. At each step, a distribution is inferred conditioned on a constraint vector, and the dynamics generated previously. Then we sample the dynamics change from this distribution and synthesize a new frame. SDVI stands out among previous studies on 4 datasets. We also infill every between frame interval of a real-world video (2fps) and connect them to create a enhanced long video of 16fps (in the full version paper). To summarize, our contributions are:

- To the best of our knowledge, it is the first stochastic model and the first study utilizes the extended frames away from the interval to solve the video infilling.
- A module *RBCConvLSTM*(see 4.1) is introduced to enforce spatial-temporal coherence.
- A spatial feature map is applied in the sampling to enables spatial independence of different regions.
- A metric LMS (see 5) is proposed to evaluate the sequence temporal coherence.

4. Model Details

As illustrated in Figure 3, SDVI consists of 3 major modules: Reference, Inference and Posterior modules. Reference module helps to propagate the constraint to each time step. Inference and the Posterior module work together to train the stochastic dynamics generation.

4.1. Reference Module

The Reference module includes an *Extractor* and a *RBCConvLSTM*. Given all the frames in \mathbf{X}_{WR} , the *Extractor* learns the momentum and output two vectors C_{start} and C_{end} . *RBCConvLSTM* outputs a dynamic constraint vector \hat{h}_t . The dynamic constraint sequence has a conditional distribution $P(\hat{h}_{S:T}|\mathbf{X}_{WR})$. We need to transfer an incomplete sequence $h_S, \mathbf{0}, \dots, h_T$ to a complete sequence $\hat{h}_S, \hat{h}_{S+1}, \dots, \hat{h}_T$. Input features of the bottom layer $h_S, \mathbf{0}, \dots, h_T$ share the same space with the output features $\hat{h}_{S:T}$ of the top layer. We add an residual connection between adjacent layers to elevate the features directly to the top. In the end, *RBCConvLSTM* combines all the three structures: the ConvLSTM, the bi-directional RNN and the residual connections (shown in Figure 4).

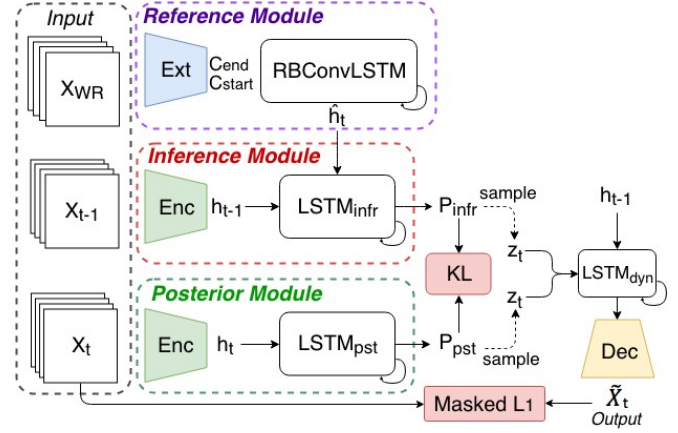


Figure 3: Training of SDVI: All green *Encoder* modules share the same weights. The blue module denotes the *Extractor* and the yellow module denotes the *Decoder*. The Reference module creates dynamic constraint \hat{h}_t for each step. At step t , the Inference module takes X_{t-1} and \hat{h}_t , while the Posterior module takes X_t . The Inference module and the Posterior module will produce different z_t and therefore different output frames \tilde{X}_t^{infr} and \tilde{X}_t^{pst} .

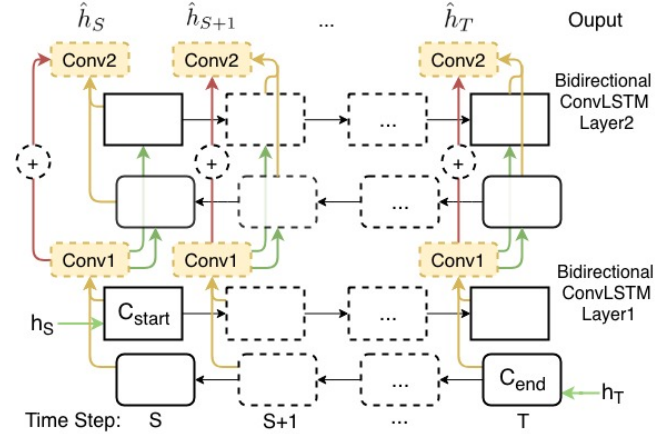


Figure 4: A two layers *RBCConvLSTM*: The initial cell states of the first layer are assigned as C_{start} and C_{end} . h_S and h_T are taken as inputs. Combined with the residuals (red arrow), each layer's outputs would go through a convolution module and become the input to the next layer. All the convolution modules in the same layer share the same weights.

4.2. Inference and Posterior Module

We extract a dynamic vector h_t from each X_t . The *LSTM_infr* takes the h_{t-1} and the dynamic constraint vector \hat{h}_t , then infers a distribution P_{infr} of the possible dynamic changes. This module resembles the prior distribution learning of stochastic prediction. The distribution of the dynamics z_t becomes $P_{infr}(z_t|X_{S:t-1}, \mathbf{X}_{WR})$.

A generated sequence $\tilde{X}_{S+1:T-1}$ can still be valid even different from the ground truth $X_{S+1:T-1}$. Therefore our model need to acquire a target distribution P_{pst} for step t , so the Inference module can be trained by matching P_{infr} to the

target. Here we expose the frame X_t to the Posterior module, so it can generate a posterior distribution $P_{pst}(z_t|X_{S:t})$ for $P_{infr}(z_t|X_{S:t-1}, \mathbf{X}_{WR})$ to match.

4.3. Training and Inference

From P_{pst} , we can sample a dynamics change vector z_t^{pst} . Along with previous generation, the $LSTM_{dyn}$ and the *Decoder* generates the \tilde{X}_t^{pst} . Separately, we also sample a vector z_t^{infr} from P_{infr} , and generate the \tilde{X}_t^{infr} in the same way. During inference, we only use the Reference module and the Inference module. The generated frame \tilde{X}_t will serve as the input of the $t + 1$ step.

4.4. Dynamic Spatial Sampling

Using the re-parameterization trick, we model P_{pst} and P_{infr} as Gaussian distributions $N_{pst}(\mu_t, \sigma_t)$ and $N_{infr}(\mu_t, \sigma_t)$. Different locations in one frame may have different levels of stochasticity. Uniformly draw a sample following the same distribution everywhere will hinder the modeling (see SDVI non-spatial in Table 1). Consequently, we introduce a spatial sampling process. Instead of using vectors [1], we use spatial feature maps for μ_t and σ_t . To get the z_t , we multiply the sampled vector on each location of σ_t , then add the μ_t on the product.

4.5. Loss Function

Reconstruction Loss To make the \tilde{X}_t^{pst} reconstruct X_t , we introduce a pixel loss $L_1(X_t, \tilde{X}_t^{pst})$. We also observe that imposing a pixel loss to the \tilde{X}_t^{infr} after the P_{infr} becoming stable can further improve the video quality.

KL Divergence Loss The $P_{pst}(z_t|X_{S:t})$ carries the dynamics from the h_t to reconstruct the X_t . Since we only use the Inference module during inference, $P_{infr}(z_t|X_{S:t-1}, \mathbf{X}_{WR})$ needs to predict the real dynamics. Therefore, we add two KL divergences between $P_{infr}(z_t|X_{S:t-1}, \mathbf{X}_{WR})$ and $P_{pst}(z_t|X_{S:t})$. Since $D_{KL}(P_{pst}||P_{infr})$ is sampled on P_{pst} , it will penalize more when P_{pst} is large and P_{infr} is small. This term will lead to a P_{infr} with higher diversity. On the other hand, $D_{KL}(P_{infr}||P_{pst})$ will make the inference more accurate when P_{infr} has large value. Here we decide to keep both terms to strike a balance between accuracy and diversity.

Full Loss Our final objective is to minimize the full loss:

$$L_C = \sum_{t=S+1}^{T-1} [\beta \cdot L_1(X_t, \tilde{X}_t^{pst}) + (1 - \beta) \cdot L_1(X_t, \tilde{X}_t^{infr}) + \alpha \cdot D_{KL}(P_{pst}||P_{infr}) + \gamma \cdot D_{KL}(P_{infr}||P_{pst})] \quad (1)$$

pixel loss 1 pixel loss 2
inclusive KL loss exclusive KL loss

The β balances the posterior and inference reconstruction, while the α and the γ determines the trade-off between the reconstruction and the similarity of the two distributions.

5. Experiments

We test SDVI on 3 datasets with stochastic dynamics: Stochastic Moving MNIST (SM-MNIST) [1], KTH Action Database [7] and BAIR robot pushing [2]. We also compare

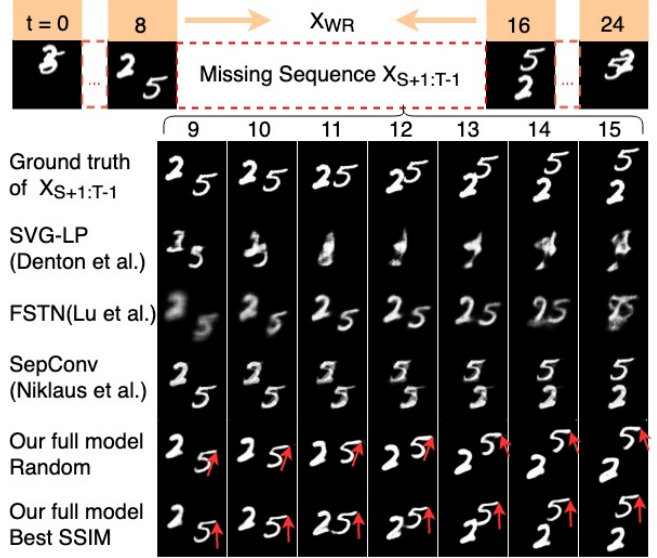


Figure 5: The digit 5 in our best sequence follows the up-ward trajectory of the ground truth. In another sampled sequence, the 5 goes upper right and then bounce upper left.

with the interpolation models on a challenging real-world dataset, UCF101 (due to space limitation, evaluation will be shown in the full version). To measure the last frame coherence, we introduce the last momentum similarity (LMS) calculated by the mean square distance between the optical flow from X_{T-1} to X_T and the optical flow from \tilde{X}_{T-1}^{infr} to X_T . Three metrics are used for evaluation: Structural similarity (SSIM), Peak Signal-to-Noise Ratio (PSNR) and LMS.

We compare our results with other state-of-the-art models: FSTN[4], a deterministic prediction model; SVG-LP[1], a stochastic prediction model; and two interpolation models SepConv[6] and SuperSloMo[3]. For FSTN and SVG, We concatenate the representation of X_T to the feature maps in each step. Ablation studies are conducted by removing the spatial sampling or the extended reference frames in \mathbf{X}_{WR} . All the evaluations are under the generation of 7 intermediate frames (more details will be included in the full paper). The Avg PSNR, SSIM and LMS over all testing frames are shown in Table 1.

5.1. Result Evaluation

SM-MINST In Figure 6, SepConv and SuperSloMo move the pixel based on the proximity: the digits 2 and 5 deform to each other since the 2 in frame 8 is closer to the 5 in frame 16. Since FSTN cannot handle the uncertainties after a bounce, the model gets confused and generates a blurry result. The SVG-LP cannot converge in this setting since it doesn't have a constraint planning module like the *RBCovLSTM* to lead the sequence to the final frame.

BAIR robot pushing dataset Although our SDVI marginally outperforms others on SSIM, the SepConv achieves the best PSNR (Table 1). In Figure 5, since the SepConv relies more on pixel proximity, the shapes of the

	SM-MNIST			BAIR			KTH			UCF101		
	PSNR	SSIM	LMS	PSNR	SSIM	LMS	PSNR	SSIM	LMS	PSNR	SSIM	LMS
SDVI full model	16.025	0.842	0.503	21.432	0.880	1.05	29.190	0.901	0.248	16.635	0.598	15.678
SDVI without 0 & 24	14.857	0.782	1.353	19.694	0.852	1.360	26.907	0.831	0.478	—	—	—
SDVI non-spatial	13.207	0.752	6.394	19.938	0.865	1.159	29.366	0.896	0.276	—	—	—
SDVI loss term 1&3	15.223	0.801	0.632	19.456	0.849	1.277	28.541	0.854	0.320	—	—	—
SVG-LP	13.543	0.741	5.393	18.648	0.846	1.891	28.131	0.883	0.539	—	—	—
FSTN	14.730	0.765	3.773	19.908	0.850	1.332	29.431	0.899	0.264	—	—	—
SepConv	14.759	0.775	2.160	21.615	0.877	1.237	29.210	0.904	0.261	15.588	0.443	20.054
SuperSloMo	13.387	0.749	2.980	—	—	—	28.756	0.893	0.270	15.657	0.471	19.757

Table 1: Metrics averaging over all 7 intermediate frames. We report the best scores among 100 sampled sequences for SDVI.

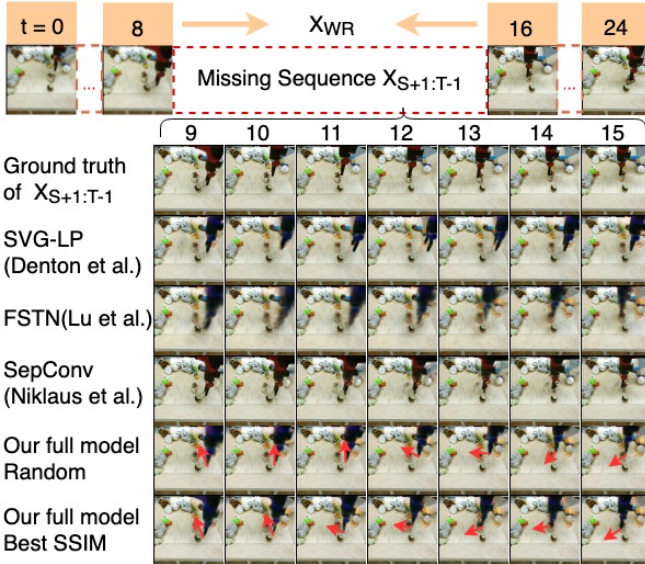


Figure 6: The best sequence follows the same movements in ground truth. In another sampled sequence, the arm firstly goes straight up and then straight left, finally downward left.

static objects are nicely preserved. However, SepConv cannot model the stochasticity while its movement is simplified to a straight sliding. Our full model can sample not only a similar sequence to the ground truth, but sequences with reasonably varied movements.

KTH Action Dataset Since most actions such as waving follow fixed patterns, the FSTN and the SepConv can achieve the best PSNR and SSIM. Illustrated in Figure 7, the result of FSTN contains blurry pixels on moving region although it keeps the static parts sharp. Our sequence with best SSIM has a similar pattern as the ground truth.

6. Conclusions

We have presented a stochastic generation framework SDVI that can infill long-term video intervals. To the best of our knowledge, it is the first study using extended reference frames and a stochastic generation model to infill long intervals in videos. Three modules are introduced to sample plausible sequences that preserves the coherence. A metric LMS is proposed to evaluate the coherence. Extensive ablation studies and comparisons demonstrate our the-state-of-the-art performance on 4 datasets.

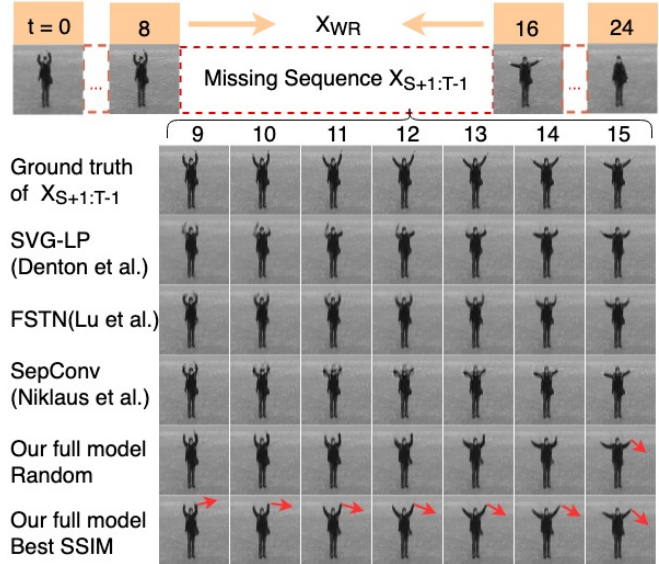


Figure 7: The best sequence keeps the arm straight. In another sample, the forearm bends first then stretches straight.

References

- [1] E. Denton and R. Fergus. Stochastic video generation with a learned prior. *arXiv preprint arXiv:1802.07687*, 2018. 3
- [2] F. Ebert, C. Finn, A. X. Lee, and S. Levine. Self-supervised visual planning with temporal skip connections. *arXiv preprint arXiv:1710.05268*, 2017. 3
- [3] H. Jiang, D. Sun, V. Jampani, M.-H. Yang, E. Learned-Miller, and J. Kautz. Super slomo: High quality estimation of multiple intermediate frames for video interpolation. *arXiv preprint arXiv:1712.00080*, 2017. 1, 3
- [4] C. Lu, M. Hirsch, and B. Schölkopf. Flexible spatio-temporal networks for video prediction. In *Proceedings of the IEEE Conference on Computer Vision and Pattern Recognition*, pages 6523–6531, 2017. 3
- [5] S. Niklaus and F. Liu. Context-aware synthesis for video frame interpolation. *arXiv preprint arXiv:1803.10967*, 2018. 1
- [6] S. Niklaus, L. Mai, and F. Liu. Video frame interpolation via adaptive convolution. In *IEEE Conference on Computer Vision and Pattern Recognition*, volume 1, page 3, 2017. 3
- [7] C. Schuldt, I. Laptev, and B. Caputo. Recognizing human actions: a local svm approach. In *Pattern Recognition, 2004. ICPR 2004. Proceedings of the 17th International Conference on*, volume 3, pages 32–36. IEEE, 2004. 3